Environ. Sci. Technol. **1998**, *32,* 3735−3742

Rapid Structure Characterization of Bacterial Aggregates

JING GUAN,[†] T. DAVID WAITE,*[,†] AND ROSE AMAL[‡]

School of Civil and Environmental Engineering and School of Chemical Engineering and Industrial Chemistry, University of New South Wales, Sydney, NSW 2052, Australia

While the structure of bacterial aggregates formed in wastewater treatment is recognized to be an important determinant of the efficiency of various processes including sedimentation, thickening, and sludge dewatering, very few methods exist for rapidly quantifying this structure. In this paper, light scattering over small angles of scatter (0.03−6.25°) is shown to produce results typical of fractal structures. Neither polydispersity effects nor multiple scattering appear to induce major problems in analysis of light scattering data for such assemblages with deviation from Rayleigh−Gans−Debye scattering behavior apparently insignificant as a result of both the low refractive index of the primary scatterers and the small angles of scatter being used. Addition of polymer results in production of larger aggregates that do exhibit effects suggestive of multiple scattering at low angles of scatter. Power law scattering is observed for such systems at larger scattering angles with a relatively ordered decrease in floc compactness with increased polymer dose (fractal dimensions reducing from around 2.2 in the absence of polymer to 1.7−1.8 in the presence of 1 wt % (dry solids) of cationic polymer). These results are supportive of the use of small-angle static light scattering for rapid determination of biosolids floc structure provided that due consideration is given to the limitations of the technique.

Introduction

Microbial aggregates or "flocs" are generated in all wastewater treatment processes whether it be in an activated sludge plant, a sequencing batch reactor, or a fixed film bioreactor. The physicochemical characteristics of these flocs will influence many of the steps involved in treatment including substrate transfer and utilization, floc formation and breakup, supernatant filtration, biosolids thickening via sedimentation and/or flotation, and biosolids dewatering. Of all the physical characteristics of bacterial aggregates, the most important are probably the floc size distribution and floc structure (*1*).

In recent years, progress has been made with regard to characterization of bacterial floc structure with the recognition that such flocs exhibit mass fractal properties (*2*−*4*). That is, the mass (M) of these aggregates may be related to their radius of gyration R_g (the standard deviation of the particles from their center of mass) by the relationship:

$$M \propto R_g^{\,D} \tag{1}$$

For linear, planar, and three-dimensionally compact objects, the exponent D will have values of 1, 2, and 3, respectively; while for porous aggregates (such as those typical of colloidal assemblages and those found in water and wastewater treatment systems), D may take a fractional value. In such cases, the exponent (which we will, for mass fractal objects, denote as D_f) is known as the "fractal dimension" which, for compact aggregates, has been found to have values in the 2.3−2.5 range (or higher if "restructuring" occurs). For "loose" aggregates, fractal dimensions in the 1.7−1.8 range are common (*5*−*7*).

An additional implication of eq 1 is that the density (ρ) of mass fractal objects is not constant but decreases as one moves away from a point on the object:

$$\rho \propto R_g^{\,D-3} \tag{2}$$

In general, the fractal dimension represents a structure that should show up at any length scale. Mass fractal objects are thus considered to exhibit "self-similarity" with respect to the spatial arrangement of the constituent particles. The concept of fractal dimension is thus only properly defined when using an asymptotic limit to infinitely small lengths. Practically, however, when considering real physical objects, there always exists a lower limiting characteristic length below which the object cannot be described as a mass fractal. In the case of aggregates, the natural lower cutoff will be the size of a few assembled primary particles (in this case bacteria) that may be considered to be the "fractal generator" for the larger assemblage.

While the fractal dimensions of colloidal aggregates have been determined using small-angle neutron and X-ray scattering and (relatively) large-angle "static" light scattering techniques (*6*, *8*−*10*), the more tedious techniques of image analysis (*11*) and settling velocity measurement (*12*) have been used for larger flocs. These methods are time-consuming and, in the case of settling velocity, require insight into the nontrivial issue of an appropriate formulation for the drag coefficient (*13*, *14*).

Static light scattering can be applied to particles in the "post-colloidal" (micron) size range, but the intensity of light scattered at small angles from the incident beam must be measured (*15*). Such an approach has been used by Risovic and Martinis (*16*) in studies of the fractal structure of micron-sized seawater particulates. In this paper, we investigate the application of small-angle static light scattering to analysis of the structure of aggregates generated in wastewater treatment processes and examine the effect on light scattering of addition of cationic polymer—an agent commonly used in wastewater treatment to modify the settling and dewatering behavior of biosolids.

Methods

Theoretical Section. *Structure Analysis by Small-Angle Light Scattering.* In a scattering experiment, a beam of light (or X-rays or neutrons) is directed onto a sample, and the scattered intensity (photon counts) is measured as a function of wave vector **q**:

$$|\mathbf{q}| = \frac{4\pi n}{\lambda} \sin\frac{\theta}{2} \tag{3}$$

where θ is the scattering angle, λ is the wavelength of the incident beam, and n is the refractive index of the medium.

* To whom correspondence should be addressed (email: d.waite@unsw.edu.au; phone: +61-2-9385 5060; fax: +61-2-9385 6139).
[†] School of Civil and Environmental Engineering.
[‡] School of Chemical Engineering and Industrial Chemistry.

10.1021/es980387u CCC: $15.00
Published on Web 10/07/1998

The quantities $\mathbf{q}\cdot\mathbf{r}_{ab}$ represents the path between light scattered at vector $\mathbf{q}$ from opposite ends of $\mathbf{r}_{ab}$, a vector describing the relative positions of two elementary scatterers a and b. The assumption that the elementary units within the scattering body (for example, the aggregate) all scatter independently (the Rayleigh−Gans−Debye approximation) leads to a simple expression for the total scattered intensity function (*17*−*19*):

$$I(\mathbf{q}) \propto \sum_a \sum_b A_a(\mathbf{q}) A_b(\mathbf{q}) \cos(\mathbf{q}\cdot\mathbf{r}_{ab}) \tag{4}$$

which is valid for nonabsorbing particles in the limit that both:

$$|m - 1| \ll 1 \tag{4a}$$

$$\frac{4\pi R}{\lambda}|m - 1| \ll 1 \tag{4b}$$

where $A_j(\mathbf{q})$ is the amplitude scattering function for scattering element j, R is the size of the scattering particle, and m is the refractive index of the particle relative to the suspending medium.

Making the assumption that the scattering particles take all orientations with equal probability, eq 4 simplifies to a scalar form (*17*)

$$I(\mathbf{q}) \propto \sum_a \sum_b A_a(\mathbf{q}) A_b(\mathbf{q}) \frac{\sin(\mathbf{q}\cdot\mathbf{r}_{ab})}{(\mathbf{q}\cdot\mathbf{r}_{ab})} \tag{5}$$

The above equation can be re-expressed in terms of a transform of a pair correlation function $c(r)$, which represents the average number of primary elements at a distance r from a given primary element

$$c(r) = \frac{1}{N}\sum_{r'}\sum_{|r|=r} \phi(r')\phi(r'+r) \tag{6}$$

where $\phi(r)$ is equal to 1 if there is a primary element at position r from an arbitrary origin and N is the total number of particles in the aggregate. For monodisperse primary particles (i.e., all $A_j(\mathbf{q})$ equal to $A(\mathbf{q})$), eq 5 becomes

$$I(\mathbf{q}) \propto [A(\mathbf{q})]^2 \int_0^\infty c(r) \frac{\sin(\mathbf{qr})}{(\mathbf{qr})}\, \mathrm{d}r \tag{7}$$

This expression may be simplified by defining the structure factor $S(\mathbf{q})$ such that $I(\mathbf{q}) \propto [A(\mathbf{q})]^2 \cdot S(\mathbf{q})$ where

$$S(\mathbf{q}) = \int_0^\infty c(r) \frac{\sin(\mathbf{qr})}{(\mathbf{qr})}\, \mathrm{d}r \tag{8}$$

$S(\mathbf{q})$ is a measure of the spatial correlations between the constituent elements of the scatterer.

If the aggregate shows fractal behavior, then the pair correlation function, $c(r)$, scales fractally (*8*) such that

$$c(r) \propto r^{D_f - 1} \tag{9}$$

In this event, the structure factor $S(\mathbf{q})$ behaves simply as

$$S(\mathbf{q}) \propto \mathbf{q}^{-D_f} \tag{10}$$

If the primary particles are small enough to behave as Rayleigh scatterers (i.e., $A(\mathbf{q})$ constant), then

$$I(\mathbf{q}) \propto \mathbf{q}^{-D_f} \tag{11}$$

This form of Q dependence of scattered light intensity is known as power law scattering, which is a signature of scattering from mass fractals (*8*).

As aggregates are typically finite in extent (defined here by their radius of gyration, R_g) and are made up of primary particles of nonzero size (say, of radius a), eq 11 can only be valid for $q \gg 1/R_g$ and $q \ll 1/a$ since for $q > 1/a$ (the Porod region), scattering will be controlled by the nature of the primary particles and not the aggregate while for $q < 1/R_g$, the aggregates will behave as Rayleigh scatterers and exhibit no angle dependence (*8*). The q range between the region where aggregates behave as Rayleigh scatterers and the region of power law behavior (the fractal region) is known as the Guinier region and depicts the onset of intraparticle interference.

The theory presented above is adequate as a description of aggregates of monosized particles only. In the more realistic case where the constituent particles take on a variety of sizes, the theory can be extended by considering the aggregate as being made up of n size classes of monosized particles and accounting for each size class and its interactions with other size classes separately (*20*). Bushell et al. (*21*) found from both experiments and simulations that polydispersity in primary particles could complicate the determination of the fractal dimension, particularly when there was a distinct difference in sizes between constituent particles. For Gaussian and narrow primary particle size distributions however, Dimon et al. (*22*) have shown that the structure factor will not be affected by polydispersity effects.

The perimeter of aggregates is rarely very sharp, and the nature of the transition from solid to liquid at the aggregate boundary may significantly affect light scattering in the Guinier regime. This has been accounted for by introducing a cutoff or "scaling" function $h(r/\xi)$ into eq 9, which governs how the density autocorrelation function terminates at the perimeter of the aggregate (*23*), i.e.

$$c(r) \propto h(r/\xi) r^{D_f - 1} \tag{12}$$

where ξ may be considered a cutoff value above which the mass distribution does not follow fractal behavior. The function $h(r/\xi)$ must have the properties that $h(r/\xi) \rightarrow 1$ when $r/\xi \ll 1$ and $h(r/\xi) = 0$ when $r/\xi > 1$. A variety of scaling functions have been used (*5*, *23*, *24*) including exponential, Gaussian, "overlapping sphere", and stretched exponential expressions. The exponential cutoff function $h(r/\xi) = \mathrm{e}^{-(r/\xi)}$ is the simplest and has the correct asymptotic behavior but been chosen for mathematical convenience and has no physical basis. It has been extensively used, although Sorensen et al. (*24*) have shown that this function is inappropriate if the system exhibits some polydispersity. Sorensen argues that the Gaussian cutoff function $h(r/\xi) = \mathrm{e}^{-(r/\xi)^2}$ is a reasonable choice (*25*), although it also has no physical basis and is, like the simple exponential, physically unrealistic in the sense that it never decays to zero as the real cutoff function should. The overlapping spheres approach (*26*) has a sound physical basis but lacks an analytic form for the structure factor. Expressions for ξ^2 and $S(\mathbf{q})$ for both exponential and Gaussian cutoff functions (which are used later in this paper) are given in Table 1.

Experimental Section. *Sample Procurement.* Samples of biosolids were obtained from the St Marys wastewater treatment plant in the western suburbs of Sydney (Australia) and, whenever possible, were analyzed on the day of collection. In some instances, samples were stored at 4 °C and analyzed after storage. As shown later in this paper, little change was observed in size or structure characteristics of the biosolids on cold storage for a few days. Three different types of wastewater biosolids were obtained: (i) a waste-activated sludge (WAS) from the aeration tank in a conven-

TABLE 1. Structure Factors and Size Cutoff Expressions for Selected Density Correlation Cutoff Functions (*24*)

$h(r/\xi)$	ξ^2	$S(q)$
$e^{-r/\xi}$	$\frac{2R_g^2}{D_f(D_f+1)}$	$\frac{\sin[(D_f-1)\tan^{-1}(q\xi)]}{(D_f-1)q\xi(1+q^2\xi^2)^{(D_f-1)/2}}$
$e^{-(r/\xi)^2}$	$\frac{4R_g^2}{D_f}$	$e^{-(qR_g)^2/D_f}\,{}_1F_1\left(\frac{3-D_f}{2}, \frac{3}{2}, \frac{(qR_g)^2}{D_f}\right)^a$

[a] ${}_1F_1$ is the hypergeometric function (*26*).

tional activated sludge process to which small amounts of ferric chloride (0.67−1.00 g of $FeCl_3$/100 g of dry solids) had been added to aid settling; (ii) a digested sludge (DS) from the biosolids digestor; and (iii) mixed liquor (ML) from the aeration tank of a biological nutrient removal (BNR) process. Mixed liquor suspended solids concentrations at the Quakers Hill plant were on the order of 7000 mg/L.

Biosolids Conditioning. While extensive characterization of unconditioned biosolids was undertaken, cationic polymer (Zetag 92, Allied Colloids (Australia) Pty. Ltd) was added in some instances to induce significant alteration in biosolids structure. In these cases, a known amount of polymer was added to the biosolids sample, and the mixture was rapidly stirred (approximately $G = 390$/s) for 0.5 min and then gently stirred ($G = 50$/s) for 1 min. The sample was then left to reach equilibrium for around 2−5 min, after which size and structure characterization was commenced. The polymer used in these studies is known to be of 10^6−10^7 molecular weight and is made up of random copolymers of acrylamide and dimethyl amino ethyl acrylate.

Size Distribution and Structure Analysis. Size distributions and structural information of bacterial assemblages were determined using a Malvern Mastersizer/E, which ascertains size by analysis of forward scattered light. The Mastersizer consists of a 5 mW He−Ne laser (632.8 nm wavelength) with 18 mm beam expansion, collimation, and spatial filtering for TEM_{00} mode transmission. The plane of polarization of the laser beam is parallel to the detector axis (vertical). The particles pass through the expanded and collimated laser beam in front of the optic lens in whose focal plane are positioned 31 photosensitive detectors. The Fourier optics can be used with 45, 100, or 300 mm lenses that allow the collection of light scattered at angles from 0.01° to 32.5°. In this work, the flocs were analyzed using the 300 mm lens enabling the collection of light scattered from 0.03° to 6.25°.

A portion of the incident light is unscattered and is brought to a focus on the detector and passes through a small aperture in the detector and out of the optical system. The total laser power passing out of the system in this way provides a measure of the "obscuration" in the measurement. An obscuration of 20% means that 20% of the incident laser has been lost to either scattering or absorption. An obscuration level of between 10 and 30% is recommended for reliable size analysis. Dilution of biosolids samples prior to size and structure analysis was required in some instances in order to obtain the recommended obscuration level. Either filtered wastewater of Milli-Q water was used for dilution purposes with the results in both cases found to be comparable.

Size distribution information was obtained using the supplied software in which Mie theory is used to develop a scattering pattern (based on scattering from spheres of refractive index 1.5) that best matches the scattering pattern of the sample under investigation. The fitting procedure is a model-independent technique, i.e., it does not constrain the volume distribution to follow some common analytical expression, such as the log-normal distribution function. The volume distributions so obtained are described using derived statistical parameters $D(M,N)$ that are defined by

$$D(M,N) = \left[\frac{\int D^M n(D)\,\mathrm{d}D}{\int D^N n(D)\,\mathrm{d}D}\right]^{1/(M-N)} = \left[\frac{\sum V_j {d_i}^{M-3}}{\sum V_i {d_i}^{N-3}}\right]^{1/(M-N)} \quad (13)$$

where V_i is the relative volume in size class i with mean class diameter d_i. In this paper $D(4,3)$, the mean diameter over the volume distribution, is used to describe mean particle size.

Information on assemblage structure was obtained by measuring the intensity of light scattered at all available detectors and plotting log intensity versus log Q (as discussed earlier). Information required to compute the angle of each detector to the incident beam as well as size and responsiveness of each detector (the so-called "magic numbers") was supplied by Malvern Instruments.

TABLE 2. Volume-Based Size Distribution Parameters Obtained for Biosolids Suspensions Using the Malvern Mastersizer/E

sample	mean diameter (SD) $D(4,3)$	distribution SD
mixed liquor (ML)	86.7 (1.7)	68.1
waste-activated sludge (WAS)	70.1 (1.4)	48.6
digested sludge (DS)	94.4 (3.6)	65.1

Results

Characteristics of Wastewater Solids. The wastewater solids obtained from the three sources appeared (through optical microscope examination) to be similar with respect to size and composition and typically consisted of aggregates of 20−50 μm in size containing a relatively diverse microbial community (Figure 1). Many of the organisms appeared to be roughly spherical of diameter less than 1 μm. Some larger filamentous organisms also appeared to be present with most organisms appearing bound relatively tightly within the flocs—presumably by extracellular polymeric material. Similar microcolonies occurring in activated sludge samples have been described by other workers (*1*, *28*).

Size distribution information for the three biosolids samples of interest obtained using the Malvern Mastersizer is summarized in Table 2 and a volume distribution obtained using the Malvern Mastersizer shown in Figure 1. While size information based on volume is the "natural" output of the Malvern Mastersizer, the relative importance of the various particles and aggregates is strongly biased toward the larger particles (given the cubed dependency of volume on particle radius).

Light Scattering Behavior. A plot of log (scattered light intensity) as a function of log (wave vector) for the activated sludge sample is shown in Figure 3. The plot is suggestive of fractal structure within the aggregates with power law dependency of I on q observed over a significant q range (from $q_{min} \cong 10^{-4.5}$ nm^{-1} to $q_{max} > 10^{-3}$ nm^{-1}). This q range indicates that we are observing power law behavior over a size range (q_{max}^{-1} to q_{min}^{-1}) of approximately 1−30 μm (i.e., over the size range spanning that from primary particles to aggregates). No angle dependency is observed for $q < 10^{-5}$ nm^{-1} (i.e., $q^{-1} > 100$ μm) since, at the small angles corresponding to these q values, light is scattered by the complete aggregates and not by the constituent particles (*29*). Very similar light scattering behavior to that shown in Figure 3 is observed for the other wastewater samples examined.

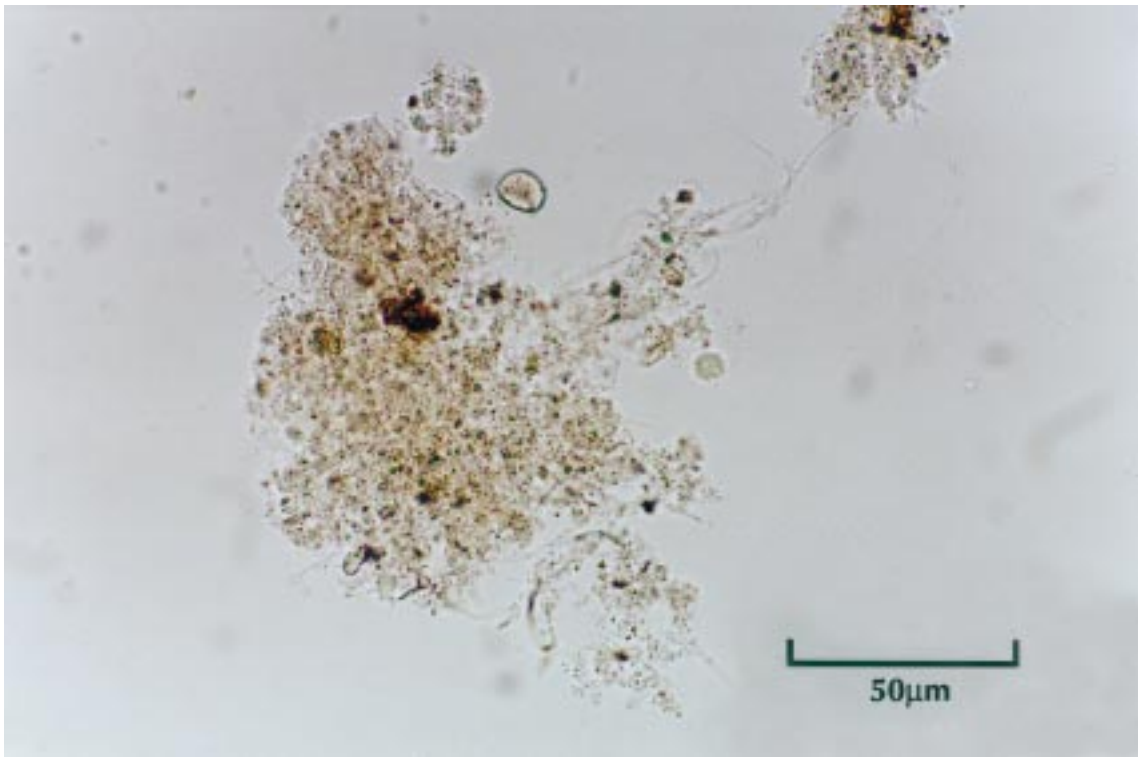

FIGURE 1. Optical microscope photograph of activated sludge floc showing constituent microorganisms.

The slope of the linear portion of the light scattering plot would be expected to provide a measure of the fractal dimension provided that (i) the Rayleigh−Gans−Debye approximation is valid (i.e., that the primary particles can be considered to be independent scatterers); (ii) the power law region is sufficiently distinct from the Guinier and Porod regions, i.e., $q \gg 1/R_g$ and $q \ll 1/a$; and (iii) polydispersity effects are insignificant. Each of these factors are briefly considered below.

As discussed earlier, the Rayleigh−Gans−Debye approximation is valid when both $|m - 1 \ll 1$ and $(4\pi R)/\lambda|m - 1| \ll 1$ are satisfied. Since the refractive index of biological solids is typically very near that of water ($m < 1.05$ (*30*)), the first condition is easily satisfied. The second condition however suggests that the RGD approximation is only valid in this instance for particle sizes significantly less than 1 μm. Early work by Kerker (*18*) and more recent studies by Farias et al. (*31*) suggest that this condition may be relaxed considerably. Comparison of absorption, total, and angular scattering cross-section predictions using both the RGD approximation and an integral equation formulation for scattering that accounts for the effects of multiple scattering and self-interaction indicate this to be particularly the case at low angles of scatter and for primary particles of low refractive index (*31*). Increasing effects of multiple scattering and interaction between particles however are to be expected as the aggregate size and compactness increase.

As indicated above, the second requirement that a distinct linear region exists between the Guinier and Porod regions is satisfied with the light scattering data exhibiting power law behavior over at least a decade of q for which $1/R_g \ll q \ll 1/a$ (assuming R_g to be on the order of at least 50 μm and a to be somewhat less than 1 μm).

Polydispersity effects may be present both in the size distribution of primary scatterers and in the cluster mass distribution. While we do not have a precise measure of the extent of polydispersity (or spread) in size of primary scatterers, visual analysis of the optical microscope plates indicates that the bulk of the particles are relatively similar in size. No evidence of the decreasing slope at high q values reported by Bushell et al. (*21*, *32*) for light scattering by highly polydisperse inorganic primary scatterers is apparent for the biosolids samples investigated here. Indeed, it is likely that any effects of polydispersity in primary scatterer size are minimized because of the low refractive index of the primary scatterers. Significant cluster mass polydispersity is recognized to lead to departures in the scattering exponent from the fractal dimension (*33*), but for the relatively narrow distributions observed here (Figure 2), polydispersity effects are expected to be insignificant (*22*).

TABLE 3. Power Law Scattering Exponent and Fractal Dimension and Size Cutoff Values for Full Scattering Equation Fits Assuming Exponential and Gaussian Density Distribution Cutoff Functions

		exponential cutoff function		Gaussian cutoff function	
sample	scattering exponent (n)[a]	D_f	R_g	D_f	R_g
ML	2.20	2.22	32.6	2.30	47.1
WAS	2.04	2.12	23.0	2.00	27.0
DS	2.20	2.24	35.2	2.10	42.0

[a] n is the number of high q data points used in the linear regression analysis.

On the basis of the above analysis, it would appear reasonable to conclude that the slope of the linear portion of the log I versus log q plots (the so-called "scattering exponent") does provide a measure of the fractal dimension of these microorganism assemblages. Scattering exponents (and standard deviations of these exponents) obtained by linear regression in the high q region of the light scattering data are shown in Table 3. Values in the 2.0−2.2 region are consistently obtained.

As outlined in the theory section, the full light scattering data set can be used to obtain an estimate of the fractal dimension (D_f) and the size cutoff value (ξ) (or radius of gyration, R_g) provided an appropriate expression for the

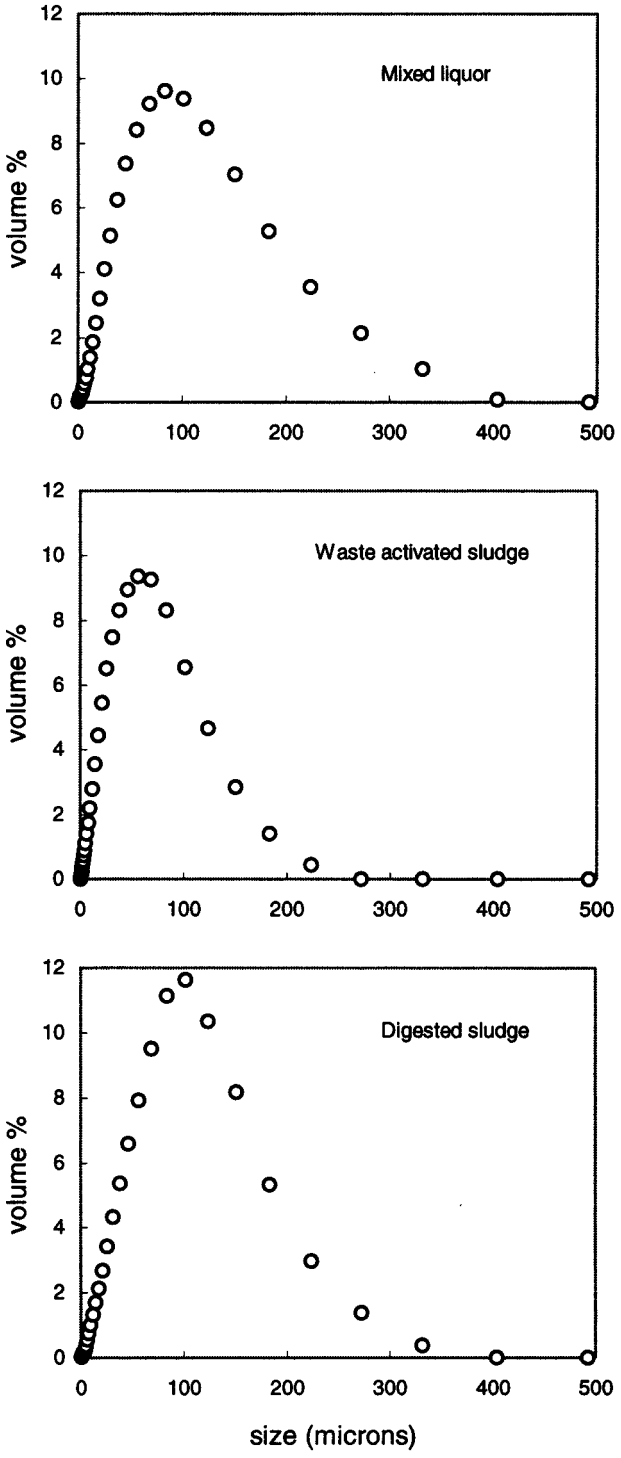

FIGURE 2. Volume-based (equivalent spherical) size distribution for mixed liquor, waste-activated sludge, and digested sludge solids obtained using the Malvern Mastersizer.

density correlation cutoff function is used. Best fit results for exponential and Gaussian cutoff functions are shown in Figure 3, and fit parameters shown in Table 3. The fractal dimension estimates obtained with both cutoff functions are similar to those estimated from the slopes of the linear portion of the log I − log q plots (the scattering exponents). This similarity is indicative of the dominance of the power law region (or lack of importance of the crossover region) in the data set and may be attributed in part to the sharpness of the interface between solid and solution at the aggregate boundary (see Figure 1). Given the sharpness of this interface, more appropriate fits are to be expected for more rapidly

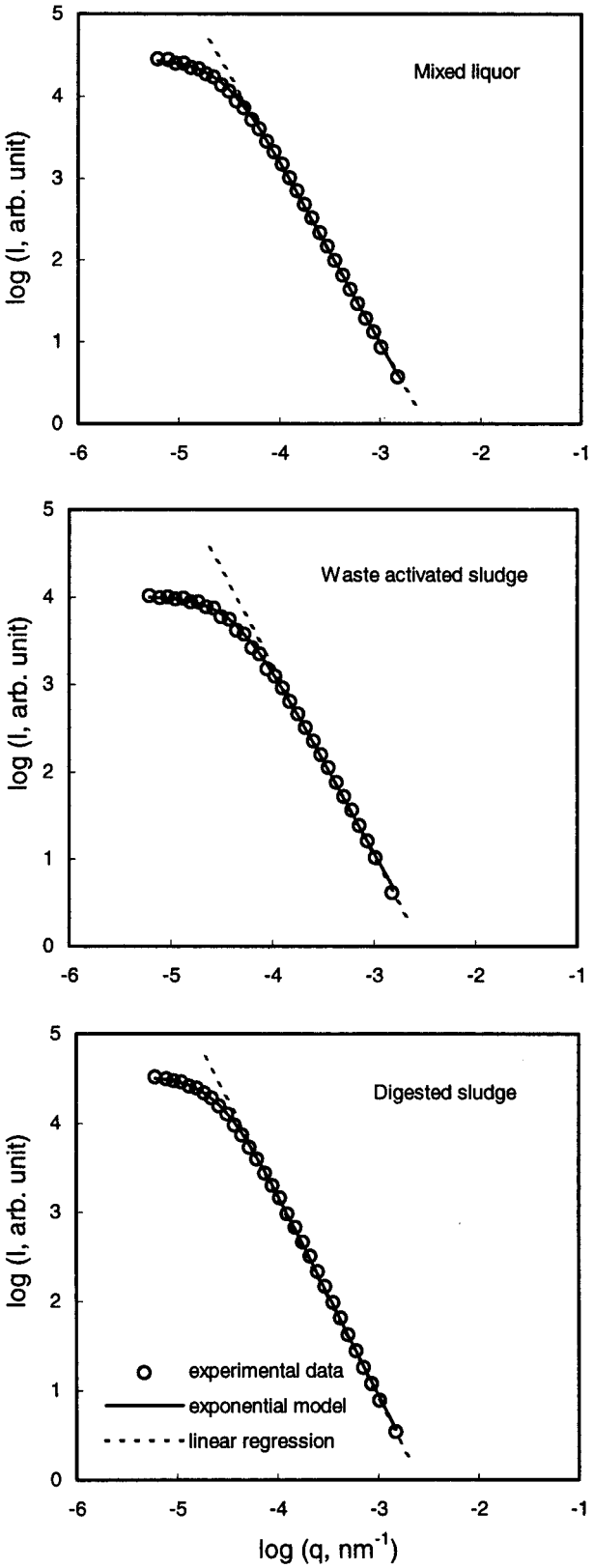

FIGURE 3. Static light scattering (log *I* versus log *q*) plot for diluted mixed liquor, waste-activated sludge, and digested sludge samples obtained using Malvern Mastersizer with 633 nm He−Ne laser. The solid and dashed lines are those obtained using structure factors derived for an exponential density correlation cutoff function and linear fit, respectively (see Table 2).

decaying cutoff functions (i.e. stretched exponential better than Gaussian better than exponential (*5*)), although a fractal dimension estimated from the slope of the power law region

TABLE 4. Effect of Increasing Dose of the Cationic Polymer Zetag 92 (as wt % of Dry Solids) on the Mean Size ($D(4,3)$) and Scattering Exponent (SE) of St Mary's Waste-Activated Sludge, Digested Sludge, and Mixed Liquor

polymer dose (%)	waste-activated sludge		digested sludge		mixed liquor	
	$D(4,3)$	SE	$D(4,3)$	SE	$D(4,3)$	SE
0	59.0	2.02	94.4	2.26	86.7	2.23
0.2	189.5	2.00	371.7	2.07	377.1	1.90
0.4	405.0	1.97	439.8	1.97	488.0	1.80
0.6	452.4	1.92	461.4	1.89	465.5	1.78
0.8	488.2	1.90	483.7	1.65	451.3	1.72
1.0	479.3	1.83	489.6	1.75	451.4	1.78

is considered quite satisfactory for the relatively large flocs considered here.

Effect of Polymer Addition. Synthetic polymers are widely used in wastewater treatment to improve the thickening, settling, and dewatering ability of biosolids. Improvements in solid−liquid separation unit process efficiencies result from the alteration induced in size and structure of the biosolids assemblages as a result of polymer addition. The impact of polymer addition on floc size is shown in Table 4 with mean diameters of the Malvern Mastersizer-derived volume distributions ($D(4,3)$ values) seen to increase to 400−500 μm for polymer contents of 0.2−0.3 wt % (of dry solids). The effect of polymer addition on angle (q) dependent light scattering behavior is shown in Figure 4a. The log I vs log q plots in the presence of polymer are markedly different to those obtained in the absence of polymer. An angle-independent scattering region at low q is no longer apparent, presumably as a result of the large size of the aggregates. Significant upward curvature in the log I vs log q plots is also evident at low q values. This increase in slope at low q may reflect increased compactness of the aggregates at larger spatial scales but, more likely, is indicative of multiple scattering and self-interaction in these large aggregates.

Scattering at higher q values exhibits reasonable power law behavior (Figure 4b). Scattering exponents obtained from this high q linear region for WAS, DS, and ML samples are given in Table 4 and show a relatively ordered decrease with increasing polymer dose.

Effect of Solids Concentration on Scattering Exponent. As noted in the experimental section, dilution of sludge samples prior to light scattering analysis was required in some instances in order to achieve a recommended obscuration level of between 10 and 30%. That such a procedure is critical in reliable estimation of structure information is evident from the results presented in Table 5 where scattering exponents are reported for obscurations of greater than 90% to less than 5%. Significant increases in scattering exponents are observed in each of the three cases examined as obscuration levels are decreased from greater than 90% to 20−30%. Highly consistent values of scattering exponents are observed at obscuration levels less than 20−30% in the "no polymer" case and for the cases with polymer present.

Effect of Floc Size on Scattering Exponent. While floc size would be expected to influence the q value at which crossover from power law behavior to zero q dependence occurs, the fractal dimension of the floc should not change provided multiple scattering and/or self-interaction effects

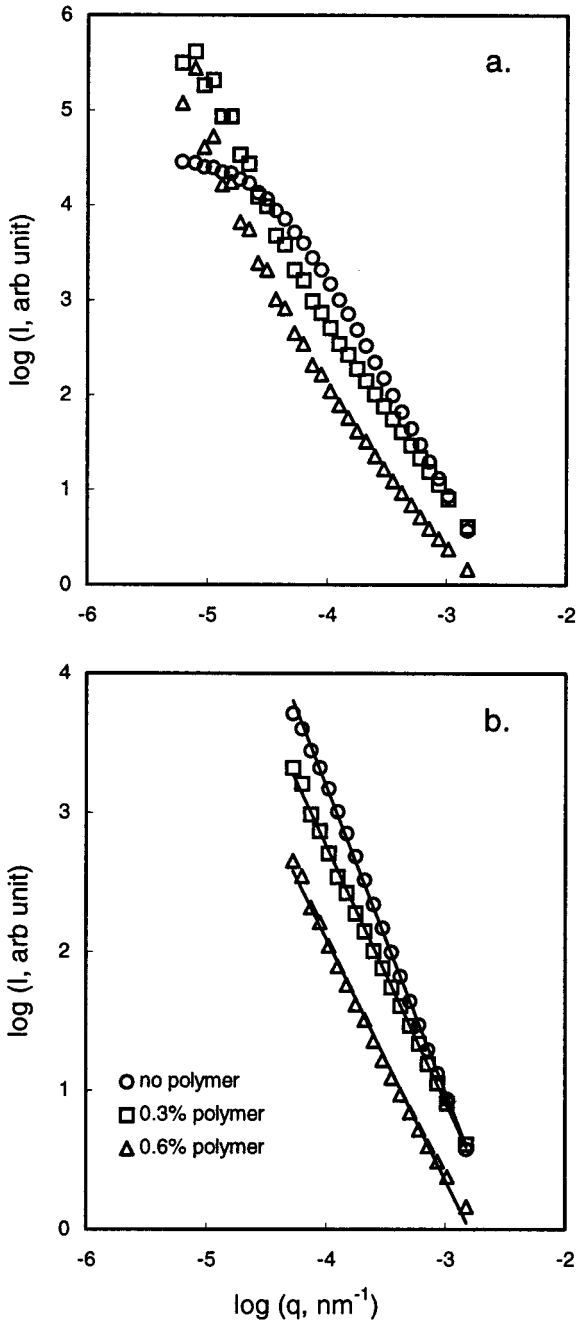

FIGURE 4. Static light scattering results (log I versus log q plots) obtained by small-angle scattering using the Malvern Mastersizer for a diluted digested sludge sample in the absence and presence of added (0.3 and 0.6%) high molecular weight cationic polymer (Allied Colloids Zetag 92). Results are shown over both (a) a wide q range and (b) limited to the high q region where log I versus log q approaches linearity.

TABLE 5. Effect of Sample Concentration (As Measured by Light Obscuration) on Scattering Exponents (SE) for St Mary's Mixed Liquor Biosolids

no polymer	obsc. (%)	93	70	33	23	18	13	7
	SE	1.81	2.02	2.18	2.21	2.22	2.23	2.25
0.1% polymer	obsc. (%)	91	53	40	22	20	10	3
	SE	1.86	2.05	2.11	2.14	2.16	2.18	2.14
0.3% polymer	obsc. (%)	93	64	45	30	17	13	3
	SE	1.71	1.82	1.84	1.85	1.87	1.87	1.85

TABLE 6. Mean Size and Scattering Exponents Obtained for Sedimentation (Size) Separated Samples of St Mary's Mixed Liquor in the Absence and Presence of Polymer (at Various Doses)

no polymer		0.1% polymer		0.2% polymer		0.3% polymer	
D(4,3)	SE	*D*(4,3)	SE	*D*(4,3)	SE	*D*(4,3)	SE
69.5 ± 2.6	2.19 ± 0.02	241.0 ± 4.8	2.09 ± 0.03	316.3 ± 6.3	1.90 ± 0.01	409.6 ± 8.2	1.83 ± 0.03
84.8 ± 1.7	2.19 ± 0.01	280.6 ± 5.6	2.10 ± 0.02	373.1 ± 7.5	1.96 ± 0.03	424.1 ± 8.5	1.84 ± 0.02
90.0 ± 4.3	2.16 ± 0.03	302.3 ± 6.0	2.12 ± 0.01	380.4 ± 7.6	1.96 ± 0.04	427.7 ± 8.6	1.85 ± 0.03
101.8 ± 3.5	2.15 ± 0.02	396.1 ± 7.9	2.05 ± 0.02	401.5 ± 8.0	1.93 ± 0.02	447.3 ± 8.9	1.85 ± 0.01

are negligible. The results presented in Table 6, which were obtained by determination of scattering exponents for mixed liquor (ML) assemblages (in the absence and presence of various polymer doses) separated according to size by sedimentation, confirm this expectation with essentially identical fractal dimensions determined for assemblages of different size but the same polymer dose. It is also noteworthy that assemblages of similar mean size but different polymer dose exhibit different scattering exponents with consistently decreasing slopes of the log I vs log q plots again observed for increasing polymer doses.

Discussion

The results presented in this paper of the scattering of light over relatively small angles from the incident direction suggest that information on the structure of aggregates made up of primary particles of biological origin (and thus of low refractive index) can be deduced from the variation of intensity with angle of scatter. In particular, the observation of power law behavior over a significant angular (or wave vector, q) range is supportive of previous suggestions that biosolid flocs develop a fractal structure over a certain size range. This apparent fractal structure of flocs is obviously limited (at small angles or q values) by the finite size of flocs (in the polymer free case) and (at relatively large angles or q values) by the finite size of the primary particles. Problems introduced as a result of deviation of light scattering behavior from that expected from Rayleigh−Gans−Debye theory appear to be small, presumably as a result of both the low primary particle refractive index and the small angles of scatter.

The fractal dimensions of 2.0−2.2 found for bacterial assemblages in the absence of added polymer are at the upper end of those calculated for activated sludge from settling velocity data by Li and Ganczarczyk (*3*) and Mitani et al. (*34*). These values may also be compared with fractal dimensions in the range of 1.7−2.7 that have been obtained by Risovic and Martinis (*16*) for assemblages of particles (most likely of biological origin) from marine systems using light scattering methods. Fractal dimensions at the lower end of this range were associated with larger assemblages believed to form via cluster−cluster aggregation while the smaller D_f values were associated with aggregates formed via a particle−cluster mechanism. The high concentrations of exocellular polymeric material that will be present in the wastewater samples studied here might be expected to modify particle−particle (or cluster−cluster) interactions over those likely to occur in more dilute environments.

Addition of cationic polymer to biosolids samples results in larger assemblages for which multiple scattering and interparticle interaction effects may well be influencing the light scattering behavior. Only in the high q regime where such effects are expected to be less severe do we see an approach to power law light scattering. In this region, a consistent decrease in scattering exponent is observed on increase in polymer concentration with values approaching 1.7 in the presence of 1 wt % (dry solids) of cationic polymer. Such behavior is suggestive of formation of increasingly open assemblages on increasing polymer dose. While caution must obviously be exercised in application of light scattering in a region where the basic tenets of RDG theory are marginal, the results obtained suggest that the technique may provide a rapid means of structure analysis of bacterial assemblages if applied wisely and with keen regard to the limitations.

Acknowledgments

The CRC for Waste Management and Pollution Control is gratefully acknowledged for provision of a Ph.D. scholarship to J.G. Dr. Heri Bustamante is thanked for his input during the early stages of this project.

Literature Cited

(1) Li, D.; Ganczarczyk, J. J. *Biotechnol. Bioeng.* **1990**, *35*, 57−65.
(2) Mandelbrot, B. B. *The Fractal Geometry of Nature*; W. H. Freeman and Co.: New York, 1983.
(3) Li, D.-H.; Ganczarczyk, J. J. *Environ. Sci. Technol.* **1989**, *23*, 1385−1389.
(4) Ganczarczyk, J. J. *Water Sci. Technol.* **1994**, *30* (8), 87−95.
(5) Lin, M. Y.; Klein, R.; Lindsay, H. M.; Weitz, D. A.; Ball, R. C.; Meakin, P. *J. Colloid Interface Sci.* **1990**, *137*, 263−280.
(6) Amal, R.; Raper, J. A.; Waite, T. D. *J. Colloid Interface Sci.* **1990**, *140*, 158−168.
(7) Logan, B. E.; Wilkinson, D. B. *Limnol. Oceanogr.* **1990**, *35*, 130−136.
(8) Schmidt, P. W. In *The Fractal Approach to Heterogeneous Chemistry: Surfaces, Colloids, Polymers*; Avnir, D., Ed.; Wiley: New York, 1989; pp 67−79.
(9) Auvray, L.; Auroy, P. In *Neutron, X-ray and Light Scattering: Introduction to an Investigative Tool for Colloidal and Polymeric Systems*; Lidner, P., Zemb, Th., Eds; North-Holland: Amsterdam, 1991; pp 199−221.
(10) Amal, R.; Gazeau, D.; Waite, T. D. *Part. Part. Syst. Charact.* **1994**, *11*, 314−315.
(11) Ganczarczyk, J. J.; Zahid, W. M.; Li, D.-H. *Water Res.* **1992**, *26*, 1695−1699.
(12) Namer, J.; Ganczarczyk, J. J. *Water Res.* **1993**, *27*, 1285−1294.
(13) Johnson, C. P.; Li, X.; Logan, B. *Environ. Sci. Technol.* **1996**, *30*, 1911−1918.
(14) Lee, D. J.; Chen, G. W.; Liao, Y. C.; Hsieh, C. C. *Water Res.* **1996**, *30*, 541−550.
(15) Jung, S.-J.; Amal, R.; Raper, J. *Part. Part. Syst. Charact.* **1995**, *12*, 274−278.
(16) Risovic, D.; Martinis, M. *J. Colloid Interface Sci.* **1996**, 182, 199−203.
(17) Guinier, A.; Fournet, G.; Walker, C. L.; Yudowitch, K. L. *Small-Angle Scattering of X-Rays*; Wiley: New York, 1955.
(18) Kerker, M. *The Scattering of Light and Other Electromagnetic Radiation*; Academic Press: New York, 1969.
(19) Bohren, C. F.; Huffman, D. R. *Absorption and Scattering of Light by Small Particles*; Wiley: New York, 1983.
(20) Salgi, P.; Rajagopalan, R. *Adv. Colloid Interface Sci.* **1993**, *43*, 169.
(21) Bushell, G.; Amal, R.; Raper, J. A. *Part. Part. Syst. Charact.* **1998**, *15*, 3.
(22) Dimon, P.; Sinha, S. K.; Weitz, D. A.; Safinya, C. R.; Smith, G. S.; Varady, W. A.; Lindsay, H. M. *Phys. Rev. Lett.* **1986**, *57*, 595.
(23) Teixera, J. *J. Appl. Crystallogr.* **1988**, *21*, 781.
(24) Sorensen, C. M.; Cai, J.; Lu, N. *Langmuir* **1992**, *8*, 2064.
(25) Sorensen, C. M. In *Surface and Colloid Chemistry*; Birdi, K. S., Ed.; CRC Press: Boca Raton, FL, 1997; Chapter 13, pp 533−558.
(26) Yanwei, Z.; Meriani, S. *J. Appl. Crystallogr.* **1994**, *27*, 782.
(27) Abramowitz, A.; Stegun, I. A. *Handbook of Mathematical Functions*; Dover: New York, 1972.

(28) Snidaro, D.; Zartarian, F.; Jorand, F.; Bottero, J.-Y.; Block, J.-C.; Manem, J. *Water Sci. Technol.* **1997**, 36, 313.
(29) Hiemenz, P. C.; Rajagopalan, R. In *Principles of Colloid and Surface Chemistry*, 3rd ed.; Marcel Dekker: New York, 1997; Chapter 5, pp 193−247.
(30) Latimer, P.; Wamble, F. *Appl. Opt.* **1982**, *21*, 2447.
(31) Farias, T. L.; Koylu, U. O.; Carvalho, M. G. *Appl. Opt.* **1996**, *35*, 6560.
(32) Bushell, G. C.; Amal, R.; Raper, J. A. *Physica A* **1996**, *233*, 859.
(33) Martin, J. E. *J. Appl. Crystallogr.* **1986**, 19, 25.
(34) Mitani, T.; Unno, H.; Akekata, T. *Jpn. Water Res.* **1983**, *6*, 69 (in Japanese).

Received for review April 16, 1998. Revised manuscript received August 3, 1998. Accepted August 27, 1998.

ES980387U